Defects in Undoped p-type CdTe Single Crystals

Tursun Ablekim, Santosh K. Swain, Jedidiah McCoy, and Kelvin G. Lynn

***Abstract*—Recently, the device performance of Cadmium Telluride (CdTe) solar cells have improved significantly. However, little progress has been made in understanding the defected structures responsible for carrier trapping, which have limited further cell efficiency improvements. In order to better understand the underlying electrical compensation mechanism, an undoped CdTe bulk crystal boule was grown from melt with Te-rich stoichiometry using the Vertical Bridgman technique, where the growth process was controlled to maximize net acceptor density. The samples prepared from the boule indicate low resistivity of 100–500 Ω·cm, and Hall measurements provided net acceptor density of (1–2) $\times$ 10^{15} cm^{-3}, which are comparable to relevant values reported from the CdTe films after $CdCl_2$ treatment. Infrared microscopy suggests there are significant amounts of secondary phases (SP's) present in the samples, where the SP's are believed to be Te inclusions and precipitates. The point defects are characterized by thermoelectric effect spectroscopy (TEES), where we observed six TEES current peaks associated with the defect levels ranging from 110 to 700 mV within the bandgap.**

***Index Terms*—Cadmium compounds, CdTe solar cells, crystal growth, doping, infrared imaging, photovoltaic cells, point defects, semiconductor growth, semiconductor impurities, II-VI semiconductor materials, TEES, thermoelectric spectroscopy.**

I. Introduction

CADMIUM TELLURIDE (CdTe) is currently one of the major semiconductor materials in the photovoltaics manufacturing industry as a low cost alternative to Si. The efficiency of CdTe thin-film solar cells reached 21% [1], competing with polycrystalline (px) Si-based solar cells. The next practical target for CdTe solar cells is ∼24%, but several challenges exist. One of the major challenges is the low material quality of the CdTe absorber layer used in the current cell fabrication process, where the hole carrier concentration (N_A) and bulk minority carrier lifetime (τ) are around 10^{13} to 10^{14} cm^{-3} and several ns, respectively [2], [3]. Improving these parameters by two orders of magnitude will raise efficiency above 24%. To accomplish this, further understanding of defect structure is necessary. Device performance can be severely impacted by trapping of electrons and holes at defects acting as recombination centers. Native defects and unintentional impurities are known to introduce localized levels to the bandgap of CdTe, influencing electrical properties.

Manuscript received June 20, 2016; revised August 14, 2016; accepted August 29, 2016. Date of current version October 19, 2016. This work was supported by the U.S. Department of Energy under Washington State University's subcontract ZEA-4-42204-01 with the National Renewable Energy Laboratory (NREL). The NREL was supported by the U.S. Department of Energy under Contract no. DE-AC36-08GO28308.

The authors are with the Center for Materials Research, School of Mechanical and Materials Engineering, Washington State University, Pullman, WA 99164-2711 USA (e-mail: tursunjan@wsu.edu; swainsk@gmail.com; jedidiah.mccoy@wsu.edu; kgl@wsu.edu).

Color versions of one or more of the figures in this paper are available online at http://ieeexplore.ieee.org.

Digital Object Identifier 10.1109/JPHOTOV.2016.2609639

Although the progress in the device efficiency is improving, little progress has been achieved in understanding the underlying mechanism of electrical compensation and the role of native defects. The p-type doping of CdTe at a very high level ($N_A > 10^{16}\,cm^{-3}$) is challenging. Although high carrier concentration and high lifetimes were recently reported with phosphorous-doped CdTe leading to open-circuit voltage greater than 1 V [4], [5], self-compensation and low activation of dopants were still observed. Native defects play a critical role in doping and compensation. In this paper, we present detailed defect characterization of undoped low resistivity CdTe single crystals providing quantitative information about native point defects. The characterization used thermoelectric effect spectroscopy (TEES) in combination with Hall effect and Infrared (IR) microscopy.

II. Experimental Details

A. Crystal Growth

A bulk CdTe crystal boule was grown from melt using the Vertical Bridgman Method. The details of the growth process are described elsewhere [6], [7]. The charge materials were 6N5 purity CdTe purchased from 5N Plus Inc., Canada. The exact stoichiometry of the starting raw material was unknown; however, it is believed to be slightly tellurium rich. The boule was grown with no component vapor pressure control during growth, where neither extra Cd nor Te was added to the melt. The resulting CdTe crystal was Te-rich due to the higher vapor pressure of Cd over Te. The growth with intended Te-rich stoichiometry was chosen for this study because, generally, as-deposited CdTe thin films in CdS/CdTe cell structures are known to be Te-rich stoichiometry. Therefore, the bulk CdTe single crystals provide model systems for defect studies without complexities of poly-crystalline thin-film characteristics such as grain boundaries and high concentrations of impurities. Although industrial manufacturing focuses on thin films, recent studies using single crystal CdTe wafers as absorber material showed improved material quality, which translated into promising cell results [5]. The point defect study using single crystal wafers will be applied to thin films as defect formation mechanism are similar but more factors such as accumulating point defects near grain boundaries should be considered.

B. Electrical Property and Purity Analysis

The impurity concentration of as-grown samples was determined at the parts per billion (ppb) atomic level using glow discharge mass spectroscopy. The N_A and resistivity (ρ) of samples were determined by room temperature Hall-effect measurements with sputtered Au contacts in Van Der Pauw configuration. The samples were 10 $\times$ 10 mm^2 and ∼1 mm thick. In

addition, variable temperature Hall measurement was performed to extract activation energy of the acceptor level.

C. IR Microscopy

IR microscopy was performed to analyze the size and distribution of the secondary phases (SP's) in crystals. The existence of Te inclusions and precipitates are known to deteriorate carrier transport. The inclusions originate from nonstoichiometric effects in melt growth and the precipitates form during crystal cooling as a result of the nucleation of native defects [8]. Inclusion size is typically around 1–50 μm, and therefore, IR microscopy is a conventional tool to characterize these defects. Only those inclusions measuring >1 μm are analyzed for our study. Depth of field (DOF) method was used to take the image of each SP. In the DOF method, a microscope's focal plane is moved through the depth of the sample.

D. Thermoelectric Effect Spectroscopy

The defect states in as-grown samples were investigated using TEES method. Samples were mechanically polished and slightly etched with a light Br/methanol solution before sputtering planar Au contacts on opposite faces of the samples with edges masked. Then, the samples were sandwiched between two planar gold plates and cooled in the dark to $\sim$20 K, where the traps were filled with a sub-band gap light emitting diode with 940 nm peak wavelength. The illumination time was 1000 s. After illumination, samples were kept in the dark for another 800 s for currents to decay to below 0.1 pA. Then, samples were heated linearly simultaneously from the top and bottom at a preset heating rate by maintaining a temperature gradient $\Delta T = 10$ K between the top and bottom surfaces to thermally release the carriers trapped at the defect states. Due to the thermoelectric effect, the temperature gradient across the sample causes a drift of the released charge carriers from the hot to the cold end. This generates a measurable current to the external circuit. The charge emanating from the traps is determined by the trap density. The temperature of trap emptying is related to the thermal ionization energy ($E_{\rm th}$) and carrier capture cross section ($\sigma_{\rm th}$) of the defect levels by

$$E_{\rm th} = k_B T_M \ln\left(\frac{\sigma_{\rm th} v_n N_c k_B T_M^2}{\beta E_{\rm th}}\right) \tag{1}$$

which can be rewritten as

$$\ln\left(\frac{T_M^2}{\beta}\right) = \frac{E_{\rm th}}{k_B T_M} - \ln\left(\frac{\sigma_{\rm th} v_n N_c k_B}{E_{\rm th}}\right) \tag{2}$$

where T_M is temperature of the current peak maximum, β is heating rate with units K/s, k_B is Boltzman constant, ν_n is carrier thermal velocity, and N_c is effective density of states in conduction band (or valence band for holes). The N_c and ν_n is given by

$$N_c = 4.829 \times 10^{15}\left[\frac{T(K)\, m^*}{m_0}\right]^{\frac{3}{2}} \text{cm}^{-3} \tag{3}$$

$$v_n = 6.743 \times 10^{5}\left[\frac{T(K)\, m_0}{m^*}\right]^{1/2} \text{cm } s^{-1}. \tag{4}$$

TABLE I
IMPURITY CONCENTRATION OF THE SAMPLE

Elements	Concentration (ppb atomic)
Na	31
Mg	94
Al	22
Si	3
P	6
S	29
Cr	14
Fe	180
Ni	61
Cu	20
Total Impurities	460

In (3) and (4), the m^* is the effective mass of electrons (or holes) and m_0 is electron rest mass. For our calculation, $m^* = 0.11m_0$ for electrons and $m^* = 0.4m_0$ for holes was used in CdTe.

The $E_{\rm th}$ and $\sigma_{\rm th}$ can be calculated by fitting temperature maxima (T_M) of current peaks with the variable heating rate method (VHR) [10], [11]. The details of theoretical and experimental aspects in TEES can be found elsewhere [12].

In VHR method, the measurement is repeated with gradually increasing heating rates, which shifts the T_M to higher temperatures. Then using (2), plotting $\ln(\frac{T_M^2}{\beta})$ versus $(\frac{1}{k_B T_M})$ will result in a straight line, where the slope is equal to the defect trap's ionization energy $E_{\rm th}$. Then, $\sigma_{\rm th}$ can be calculated from the intersection of the fitted line with y-axis. Because electrons and holes have a different mass, the $\sigma_{\rm th}$ will be different for electron and hole traps.

TEES method is a robust technique to investigate point defects in semiconductors, but it assumes several pre-conditions to accurately extract defect information.

1) Samples are high resistivity, preferably above 10^8 Ω·cm.
2) Contacts are Ohmic. With near-perfect Ohmic contact, positive and negative current peaks in the TEES spectra correspond to hole and electron traps, respectively.
3) Hole and electron mobility in samples are similar.
4) Data analysis assumes no retrapping of carriers after emanating from the traps.

However, in the case of CdTe for photovoltaics, these conditions depart from ideal. Making an Ohmic contact to CdTe is a well-known problem. In nonideal Ohmic contacts, carriers have higher chances of being collected from one side than the other. In most of the p-type CdTe samples, we observed currents were either all positive or negative. Therefore, the sign of current peaks may not necessarily correspond to the trap types as long as testing conditions remain imperfect.

III. RESULTS AND DISCUSSIONS

Table I outlines major impurity levels detected in the sample. The major impurity of interest, Cl, was not detected. Total impurities found in the samples are under 500 ppb, which are several orders of magnitude lower than reported values used in similar study [13]. The concentration of Cu and Na levels are only around 20 and 31 ppb, which are not believed to create significant defect levels to impact crystal properties.

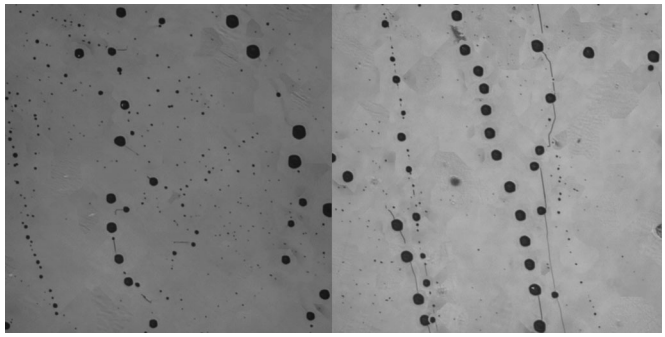

Fig. 1. SP's from two locations of a sample observed by IR microscopy with an analysis area of $0.5 \times 0.5\,\text{mm}^2$.

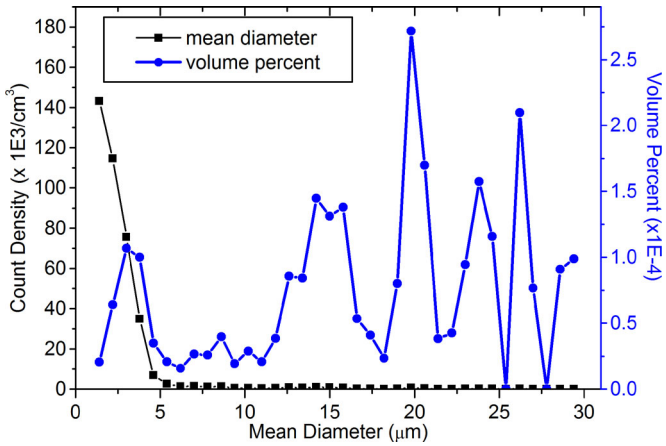

Fig. 2. Distribution of Te-inclusions with mean diameter $>1\ \mu$m. The analysis volume is $2.5 \times 2.5 \times 2.16\,\text{mm}^3$. The total count density is 390 943 cm^{-3}, and total volume percent is 0.00268%.

Hall measurements show that the samples are p-type with $N_A = (1-2) \times 10^{15}\,\text{cm}^{-3}$ and $\rho = (100-500)\,\Omega \cdot \text{cm}$. Tested samples were cut from different locations of the boule. It can be seen that the N_A is on the higher side of reported values from CdTe films after $CdCl_2$ treatment.

Analysis of IR microscopy from samples from different locations of the boule showed significant amount of SP's $> 1\ \mu$m, which are believed to be Te-inclusions. Fig. 1 shows IR images for two samples, where the dark objects are IR opaque SP's. The size of dark objects is related to the cross-section of SP's.

The distribution of SP's was further analyzed by counting the SP's and measuring the mean diameter with an image processing software, where the results are shown in Fig. 2. We report the count density and volume percent as a function of the mean diameter of SP's. The mean diameters are calculated by approximating the inclusions to spherical shapes and then taking the statistical mean over the range of the distribution of diameters. The counts density of inclusions with smaller sizes (1–4 μm) are in the range of 10 000–100 000 cm^{-3} but accounts for volume percent in the crystal. The counts of larger inclusions (5–30 μm) are on the order a few thousand, but the volume percent is higher.

In general, SP's can impact opto-electrical properties of the material directly via dislocation field surrounding it or indirectly through gettering impurities near the inclusion site. The impact of SP's on device performance has been studied intensively in

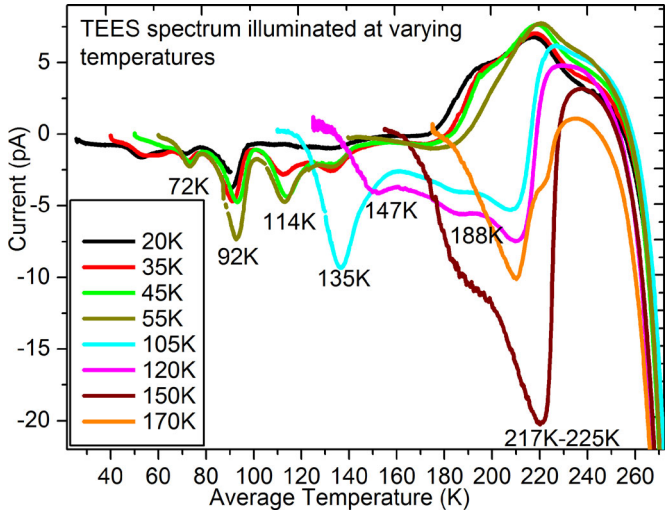

Fig. 3. TEES spectrum of the CdTe sample illuminated at different temperatures specified in the legend. The sample is illuminated by LED source with 940 nm peak wavelength. 8 V bias was applied to the sample during illumination; $\Delta T = 10\,\text{K}$ and heating rate is 0.20 K/s.

detector application of CdZnTe but few reports are available in the PV device performance. A study of correlating SP's with bulk lifetime of CdTe, and the resulting PV device performance will be an interesting direction to investigate.

The TEES spectra obtained from the sample illuminated at varying temperatures are shown in Fig. 3. Generally, in TEES method, data is collected and analyzed by illuminating the sample at low temperatures (5–30 K). However, as shown in Fig. 3, there were no peaks observed from 100 to 180 K when the sample was illuminated at 20 K. When illuminated at 35 K, two peaks are clearly observed, respectively, at 114 and 135 K, suggesting that peaks could be hidden. In order to acquire full information of peaks and peak locations, the measurement was continued by illuminating the sample from 45 to 150 K so that hidden peaks could be observed (if any). Illumination at 55 K confirms a strong peak at 92 K and a clear, well-formed peak at 114 K. It also reveals the existence of a peak at 135 K. Illumination at 105 K confirms the 135 K peak.

With various setups and scans illuminating at different temperatures, we confirmed that there are six peaks present in the sample, which are located at temperatures 72, 92, 114, 135, 188, and 217 K at a 0.20 K/s heating rate. The number of peaks and peak locations were also confirmed by flipping the sample. The peak location may move to either direction about ± 5 K at different setups. There is an ambiguity of a possible peak at around 145–150 K, but careful data analysis suggests it is most likely a shift of 135 K peak because it was not observed with any setups when illuminated below110 K. When illumination is at or close to a peak location, the peak tends to shift to higher temperatures due to partial filling of the traps. On the other hand, even if there is a peak at 145–150 K, considering the failure to observe the peak with different samples and setups, the trap density corresponding to this possible peak can be considered negligible.

Next, we performed VHR analysis to extract ionization energies and capture cross sections of the defects associated with the peaks observed. Two setups were employed separately to

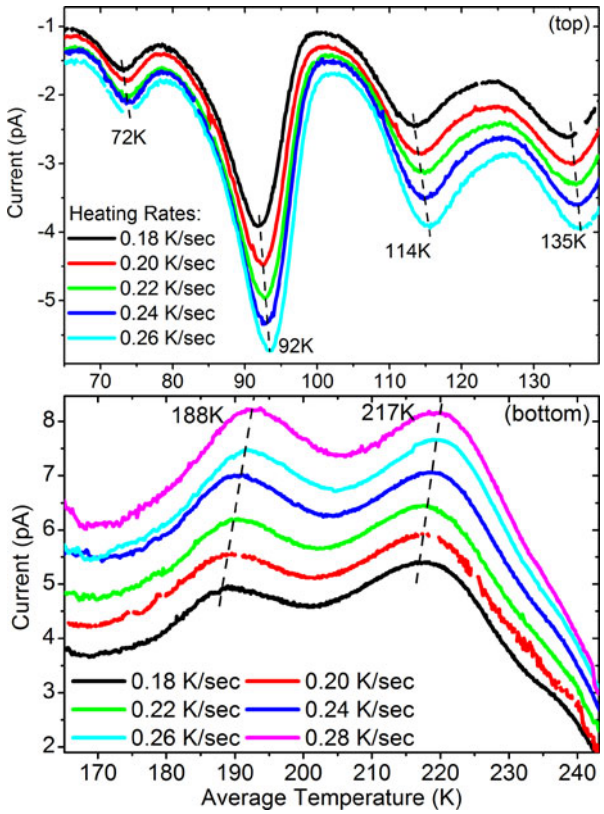

Fig. 4. VHR TEES spectrum for (top) peaks at 72, 92, 114, and 135 K; the sample is illuminated at 35 K and (bottom) peaks at 188 and 217 K, where the sample is illuminated at 120 K. The dashed lines are guides to the eyes only to show the shifting of the peaks at gradually increased heating rates. Peak positions are labeled with respect to 0.20 K/s heating rate.

acquire reproducible VHR spectra ensuring each peak was well formed. The resulting VHR spectra are shown in the top and bottom figures in Fig. 4. The top figure illustrates the first four peaks at 72, 92, 114, and 135 K, respectively, where the data were acquired with sample illuminated at 35 K. The bottom figure illustrates the peaks at 188 and 217 K, respectively, where the sample was illuminated at 120 K. Then, for calculation, every peak at each heating rate was analyzed, and temperature locations of peaks were extracted either by looking at the highest peak position if the peak is well formed or by fitting the peak with a Lorentzian function. For each peak, at least three curve fittings were performed to identify peak location. When peaks were broad, such as 188 and 217 K peaks, more than five fittings were performed.

Here, we show the extraction of $E_{\rm th}$ and $\sigma_{\rm th}$ parameters for the 92 K peak in Fig. 4. Five heating rates were employed in this VHR experiment varying from 0.18 to 0.26 K/s with 0.02 K/s increment. With increasing heating rates, peak maxima (T_M) positions shift toward higher temperatures producing higher current. Exact location of the peaks at each heating rates were analyzed and extracted by fitting to a Lorentzian function. Then, these data points were plotted by $\ln(\frac{T_M^2}{\beta})$ versus $(\frac{1}{k_B T_M})$ and fitted to a straight line, as shown in Fig. 5. This routine of fitting resulted in a slope of 0.18923, which corresponds to the $E_{\rm th}$ of 189 meV. The cross section of the straight line with

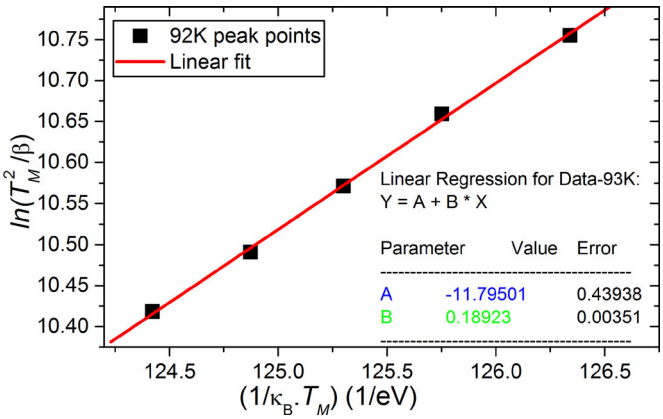

Fig. 5. Extraction of $E_{\rm th}$ by linear fitting using peak positions and heating rates.

TABLE II
CALCULATED THERMAL IONIZATION ENERGY AND TRAPPING CROSS SECTIONS

Peaks T(K)	E_{th} range (meV)	Mean E_{th} (meV)	σ_{th} (cm^{-2})
72 K	107 – 127	118 ± 7	$(0.9 \pm 1.3) \times 10^{-17}$
92 K	178 – 197	191 ± 13	$(4.1 \pm 5.1) \times 10^{-16}$
114 K	220 – 232	225 ± 11	$(8.4 \pm 4.5) \times 10^{-17}$
135 K	320 – 331	327 ± 7	$(1.7 \pm 0.6) \times 10^{-15}$
188 K	472 – 506	489 ± 22	$(6.3 \pm 5.2) \times 10^{-14}$
217 K	690 – 727	706 ± 22	$(9.4 \pm 7.4) \times 10^{-12}$

y-axis, –11.79501, is related to $E_{\rm th}$ by $\ln(\frac{\sigma_{\rm th} v_n N_c k_B}{E_{\rm th}})$, from which the $\sigma_{\rm th}$ is calculated.

The result of extracted thermal ionization energies and carrier capture cross sections for all peaks are listed in Table II. A small uncertainty in peak fittings, e.g., $\pm$0.02 K, can translate into bigger uncertainties in corresponding $E_{\rm th}$ and $\sigma_{\rm th}$ values: up to 15% and 50%, respectively. Therefore, for the thermal ionization energies, we report a range and a mean value for clarity. Because the effective mass of electrons and holes are different, they yield different values for capture cross sections.

The peak at 72 K has ionization energy around 118 ± 7 meV and trapping cross sections of $(0.9 \pm 1.3) \times 10^{-17}$ cm^{-2}. The intensity of the peak is small compared with all other peaks in the spectrum. Considering that the CdTe crystal is Te-rich stoichiometry, this peak is most likely associated with Te vacancies ($V_{\rm Te}$). Earlier studies [14] have proposed that a $V_{\rm Te}$ defect is a main deep-level defect in CdTe. However, recent reports suggest Te vacancies are shallow donors which can form in Te-rich conditions due to very low formation energy [15]. The predicted transition energies are $\sim$130 meV below the conduction band, which is very close to our experimental value of 118 ± 7 meV. Based on the observation and the close agreement with recent publications, we assign this defect to Te vacancies.

The peak at 92 K is a strong peak with resulting ionization energy and capture cross section 191 ± 13 meV and $(4.1 \pm 5.1) \times 10^{-16}$ cm^{-2}, respectively. The peak is very prominent in that it is the highest peak among all the shallow and mid-gap defect peaks associated with peaks at 72, 114, and 135 K. The peaks at 188 and 217 K are due to deep level defects. Considering the CdTe crystal is p-type contributed by

intentionally created V_{Cd} type acceptors, and the 92 K peak is very prominent, we associate this peak with cadmium vacancies. In CdTe, Cd vacancies act as acceptors with two ionization energy levels, the first ionization state $V_{\mathrm{Cd}}^{(0/-1)}$ and the second ionization state $V_{\mathrm{Cd}}^{(-1/-2)}$ have been reported. The literature [14], [16]–[18] reports around 110–140 meV for the $V_{\mathrm{Cd}}^{(0/-1)}$. In contrast, the energy levels of isolated $V_{\mathrm{Cd}}^{(-1/-2)}$ has long been debated. Researchers reported a wide range of values such as 0.65–0.73 eV [19], [20], 0.36–0.47 eV [15], [21], [22], and 0.20–0.23 eV [14], [23]. In addition, it is difficult to separate out the ionization level with the TEES data. The peak at 92 K is most likely due to $V_{\mathrm{Cd}}^{(-1/-2)}$ level.

The peak at 114 K has ionization energies of 225 ± 11 meV and capture cross sections with $(8.4 \pm 4.5) \times 10^{-17}\,\mathrm{cm}^{-2}$. The intensity of the peak is smaller than the 92 K peak. While no particular point defect associated with this peak has been confirmed yet, we have observed that this peak is very week in Cd-rich grown CdTe crystals. The dislocation density (DD) is related to growth stoichiometry, where a significant amount of DD is expected in Te-rich CdTe crystals. Studies have revealed that dislocations are prevalent in CdTe crystals, even in the best epitaxially grown CdTe films. The density of grown-in dislocations in CdTe typically is in the order of magnitude of 10^5–$10^6\,\mathrm{cm}^{-2}$. Like point defects, dislocations can potentially limit device performances. While not confirmative, studies have shown that introduction of dislocations in CdTe produce a deep level of 0.7 eV [24] below the conduction band or a shallow to mid-level of 0.17 ± 0.02 eV [25]. We tentatively assign the peak at 114 K to dislocations, but further confirmation will be needed.

The peak at 135 K has an ionization energy of 327 ± 7 meV and capture cross section of $(1.7 \pm 0.6) \times 10^{-15}\,\mathrm{cm}^{-2}$. Considering the growth stoichiometry and recent theoretical work which suggested Te interstitials are the most important defects that can be present and impact crystal properties, this peak is likely to be associated with Te interstitials.

The peaks at 188 and 217 K appear to be deep level defects with ionization energies 489 ± 22 and 706 ± 22 meV, respectively. They also produce large trapping cross sections on the order of $10^{-14}\,\mathrm{cm}^{-2}$ and $10^{-12}\,\mathrm{cm}^{-2}$. We tentatively assign 188 and 217 K peaks to Te antisites (Te_{Cd}) and complex defects $V_{Cd} - Te_{Cd}$, respectively.

IV. Conclusion

CdTe single crystals grown from melt in a Te-rich stoichiometry shows a p-type behavior comparable to $CdCl_2$ treated CdTe films. With TEES analysis, six defect levels ranging from 118 to 706 mV were identified and the possible nature of these levels is discussed. More experimental investigations, such as postannealing in varying stoichiometry and vapor pressures are needed to confirm the suggested assignment.

References

[1] M. A. Green, K. Emery, Y. Hishikawa, W. Warta, and E. D. Dunlop, "Solar cell efficiency tables (version 47)," *Progr. Photovolt.: Res. Appl.*, vol. 24, pp. 3–11, 2016.

[2] L. Kranz *et al.*, "Tailoring impurity distribution in polycrystalline CdTe Solar Cells for enhanced minority carrier lifetime," *Adv. Energy Mater.*, vol. 4, no. 7, pp. 1301400, 2014.

[3] W. K. Metzger, D. Albin, M. J. Romero, P. Dippo, and M. Young, "CdCl2 treatment, S diffusion, and recombination in polycrystalline CdTe," *J. Appl. Phys.*, vol. 99, 2006, Art. no. 103703.

[4] T. Ablekim, S. K. Swain, D. Kuciauskas, N. S. Parmar, and K. G. Lynn, "Fabrication of single-crystal solar cells from phosphorous-doped CdTe wafer," in *Proc. IEEE 42nd Photovolt. Spec. Conf.*, 2015, pp. 1–4.

[5] J. M. Burst *et al.*, "CdTe solar cells with open-circuit voltage breaking the 1 V barrier," *Nature Energy*, vol. 1, 2016, Art. no. 16015.

[6] S. K. Swain *et al.*, "Bulk growth of uniform and near stoichiometric cadmium telluride," *J. Crystal Growth*, vol. 389, pp. 134–138, Mar. 2014.

[7] S. K. Swain, K. A. Jones, A. Datta, and K. G. Lynn, "Study of different cool down schemes during the crystal growth of detector grade CdZnTe," *IEEE Trans. Nucl. Sci.*, vol. 58, no. 5, pp. 2341–2345, Oct. 2011.

[8] P. Rudolph, "Non-stoichiometry related defects at the melt growth of semiconductor compound crystals—A review," *Crystal Res. Technol.*, vol. 38, pp. 542–554, 2003.

[9] D. Kuciauskas *et al.*, "Minority carrier lifetime analysis in the bulk of thin-film absorbers using subbandgap (two-photon) excitation," *IEEE J. Photovolt.*, vol. 3, no. 4, pp. 1319–1324, Oct. 2013.

[10] R. H. Bube, *Photoconductivity of Solids*. New York, NY, USA: Wiley, 1960.

[11] R. Soundararajan and K. G. Lynn, "Effects of excess tellurium and growth parameters on the band gap defect levels in CdxZn1−xTe," *J. Appl. Phys.*, vol. 112, 2012, Art. no. 073111.

[12] B. Šantić and U. Desnica, "Thermoelectric effect spectroscopy of deep levels—Application to semi-insulating GaAs," *Appl. Phys. Lett.*, vol. 56, pp. 2636–2638, 1990.

[13] D. S. Albin *et al.*, "Cd-rich and Te-rich low-temperature photoluminescence in cadmium telluride," *Appl. Phys. Lett.*, vol. 104, Mar. 2014, Art. no. 092109.

[14] S. H. Wei and S. B. Zhang, "Chemical trends of defect formation and doping limit in II-VI semiconductors: The case of CdTe," *Phys. Rev. B*, vol. 66, Oct. 2002, Art. no. 155211.

[15] J. Ma *et al.*, "Dependence of the minority-carrier lifetime on the stoichiometry of CdTe using time-resolved photoluminescence and first-principles calculations," *Phys. Rev. Lett.*, vol. 111, Aug. 2013, Art. no. 067402.

[16] A. Castaldini, A. Cavallini, B. Fraboni, P. Fernandez, and J. Piqueras, "Deep energy levels in CdTe and CdZnTe," *J. Appl. Phys.*, vol. 83, pp. 2121–2126, Feb. 1998.

[17] A. Carvalho, S. Öberg, and P. R. Briddon, "Intrinsic defect complexes in CdTe and ZnTe," *Thin Solid Films*, vol. 519, pp. 7468–7471, Aug. 31, 2011.

[18] R. Soundararajan, K. Lynn, S. Awadallah, C. Szeles, and S.-H. Wei, "Study of defect levels in CdTe using thermoelectric effect spectroscopy," *J. Electron. Mater.*, vol. 35, pp. 1333–1340, Jun. 1, 2006.

[19] P. Höschl, R. Grill, J. Franc, P. Moravec, and E. Belas, "Native defect equilibrium in semi-insulating CdTe(Cl)," *Mater. Sci. Eng.: B*, vol. 16, pp. 215–218, Jan. 30, 1993.

[20] N. Krsmanovic *et al.*, "Electrical compensation in CdTe and Cd0.9Zn0.1Te by intrinsic defects," *Phys. Rev. B*, vol. 62, pp. R16279–R16282, Dec. 15, 2000.

[21] P. Emanuelsson, P. Omling, B. K. Meyer, M. Wienecke, and M. Schenk, "Identification of the cadmium vacancy in CdTe by electron paramagnetic resonance," *Phys. Rev. B*, vol. 47, pp. 15578–15580, Jun. 15, 1993.

[22] C. Szeles, Y. Y. Shan, K. G. Lynn, A. R. Moodenbaugh, and E. E. Eissler, "Trapping properties of cadmium vacancies in Cd1−xZnxTe," *Phys. Rev. B*, vol. 55, pp. 6945–6949, Mar. 15, 1997.

[23] U. Reislöhner, J. Grillenberger, and W. Witthuhn, "Band-gap level of the cadmium vacancy in CdTe," *J. Crystal Growth*, vols. 184/185, pp. 1160–1164, Feb. 2, 1998.

[24] H. Leipner, J. Schreiber, H. Uniewski, and S. Hildebrandt, "Dislocation luminescence in cadmium telluride," *Scanning Microsc.*, vol. 12, pp. 149–160, 1998.

[25] S. A. Awadalla, A. W. Hunt, R. B. Tjossem, K. G. Lynn, C. Szeles, and M. Bliss, "Evidence for dislocations or related defects present in CdTe and Cd1-xZnxTe crystals," *Proc. SPIE*, vol. 4507, pp. 264–272, 2001.

Authors' photographs and biographies not available at the time of publication.